Article

MULTI-SCALE MODELING AND STUDY OF AEROSOL GROWTH ON AMINE-BASED CO_2 CAPTURE ABSORBER

Jia-Lin Kang[a]*, Kuan-Ting Liu[b], David Shan-Hill Wong[b*], Shi-Shang Jang[b*] and De-Hao Tsai[b]

[a]Department of Chemical and Material Engineering, National Yunlin University of Science and Technology, Yunlin, 64002, Taiwan, ROC

[b]Department of Chemical Engineering, National Tsing Hua University, Hsinchu 30013, Taiwan, ROC June 2020

* Correspondence: Corresponding authors: jlkang@yuntech.edu.tw

Abstract

In this study, a monoethanolamine aerosol growth model was developed to investigate the aerosol growth factor. Interactions among the internal conditions in an absorber were considered in this aerosol model. Additionally, an experiment was conducted to measure aerosol particle size, for collecting in-house validation data. Sucrose was used as the aerosol nuclei instead of sulfuric acid to prevent the corrosion of equipment used in the experiment. Experimental results showed that the outlet aerosol sizes increased to the same size regardless of the sucrose concentrations. The aerosol growth model was validated using the in-house experimental data. The aerosol growth model efficiently predicted the aerosol size. For investigating aerosol growth effects, particle number concentration was determined to be the primary factor affecting aerosol growth and amine emissions. When the particle number concentration increased, the aerosol size decreased, whereas the MEA emission increased.

Keywords: aerosol; amine emission; CO_2 capture; absorber; particle number concentration

1. Introduction

The chemical capture and absorption of post-combustion CO_2 by chemical solvents have been commercialized as a technology and amine solution has been used as the commercial absorbent to capture CO_2. Due to the developments and scaling up of technology, there has been an increase in challenges associated with the use of chemical solvents. One such challenge is the leakage of amine solution, which is known to harm humans and the environment. Thitakamol et al. (2007) reported the emission of monoethanolamine (MEA) vapor to be 0.11–0.72 kg/tonne CO_2 with a removal capacity of 1000 tonne CO_2/day, using 30 wt% MEA. This significant amount of amine emission led to an increase in the operating costs. Furthermore, the exhausted amine reacted with No_x in the flue gas to form nitrosamines (Dave et al., 2010; Fine et al., 2013). Kamijo et al. (2013) compared amine emission between MEA and KS-1™ solvents; they reported that MEA and KS-1™ emissions were 0.8–67.5 and 0.4–23.2 ppmv, respectively, based on the fuel gas containing 0–3 ppmv of SO_3. Their study also revealed that amine was entrained by aerosol, which was produced from SO_3. A pilot plant at Karlsruhe Institute of Technology conducted a series of aerosol studies and estimated gas-particle growth mechanism (Brachert et al., 2014; Khakharia et al., 2015; Mertens et al., 2014). Mertens et al. (2014) found that the sizes of H_2SO_4 aerosols, with 10^8 #/cm^3 particle number concentration (PNC), entering the absorber were smaller than 0.2 μm. The final aerosol size at the outlet of the absorber was observed to grow to 0.5–2 μm. Brachert et al. (2014) used a condensation particle counter and electrical low-pressure impactor (ELPI$^+$) to measure sulfuric acid aerosols and found that ELPI+ could observe the size of the volatile aerosol. They also observed that higher sulfuric acid concentration increased the aerosol size; however, it did not affect the PNC. Khakharia et al. (2015) reported that

amine solvents could condense on the surface of nuclei and get carried away to the atmosphere. SO_3/H_2SO_4 nuclei formed the aerosols. It was indicated that any SO_3 present in the flue gas can rapidly react with water vapor to form H_2SO_4 vapor, which can quickly condense and produce aerosol particles. These result pointed out three factors that affect amine emissions by aerosols during the CO_2 capture process: (i) PNC, (ii) supersaturation, and (iii) reactivity of amine. It has been observed that when the PNC of H_2SO_4 aerosol increased by 1.6 times, the amount of MEA emission doubled. It was inferred that the PNC of H_2SO_4 aerosol was the main factor affecting amine emission. Furthermore, aerosols with diameters bigger than 10 μm have been observed to be removed by inertial impaction (Bradie and Dickson, 1969; El-Dessouky et al., 2000), however, aerosols in the absorber have been found to have diameters smaller than 3 μm due to the limitation of absorber operating conditions. Thus, predicting aerosol growth was considered to be essential for removing the aerosol using the CO_2 capture process.

To predict aerosol growth, Fulk et al. (2015) presented a model combining the Aspen Plus absorber model and MATLAB to describe the amine aerosol growth for CO_2 absorption using piperazine solvent. Their results revealed that increasing the vapor pressure of water contributed to a faster growth of the aerosol. However, they only considered the mass transfer of the gas and aerosol interface; thus, their model was unable to describe the effect of changes in amine in the gas phase. Moreover, this model was not validated using experimental data.

Thus, the purpose of this study was to investigate the aerosol growth effect factors using a model developed for the amine aerosol growth on CO_2 absorption using an MEA solvent. The amine aerosol growth and gas phase effect were simultaneously considered in the model and were subsequently validated using the in-house experimental data. The purpose of the aerosol growth model was to investigate the final size and MEA emission at the outlet of the absorber by examining various PNCs and initial sizes.

2. Modeling Approach

2.1. Data extraction from the absorber model

This study adopted a multiscale modeling, i.e., meter-scale for absorbers and micron-scale for aerosol droplets, because the difference in the scale between the absorber columns and aerosol droplets was higher than six orders of magnitudes. When the two models were simulated on the micron-scale, the number of integration steps increased, leading to a significantly high computation cost. However, when the two models were simulated in the meter-scale, the model of the aerosol droplets could not be integrated because of longer integration steps. Thus, to implement the simulation of the two different scales, Aspen Plus and gPROMS coupling was used to construct the multiscale modeling. Aspen Plus was used for simulating absorber profiles and gPROMS was used for building an amine aerosol growth model. Figure 1 shows the method adopted for connecting Aspen Plus and gPROMS. Microsoft Excel was used as the connecting interface between Aspen Plus and gRPOMS. On Aspen Plus side, Visual Basic for Applications (VBA) was used for extracting the data from the absorber from Aspen Plus to Excel. The extracted data were gas and liquid temperatures, gas and liquid mole fractions, liquid holdup, gas-liquid interfacial area, and mass transfer coefficients. On gPROMS side, Foreign Objects, which is a macro in Excel provided by gPROMS, sent or received the parameters between Excel and gPROMS. In this study, the amine aerosol growth model sent the position of the aerosol in the absorber to receive the corresponding data of the absorber.

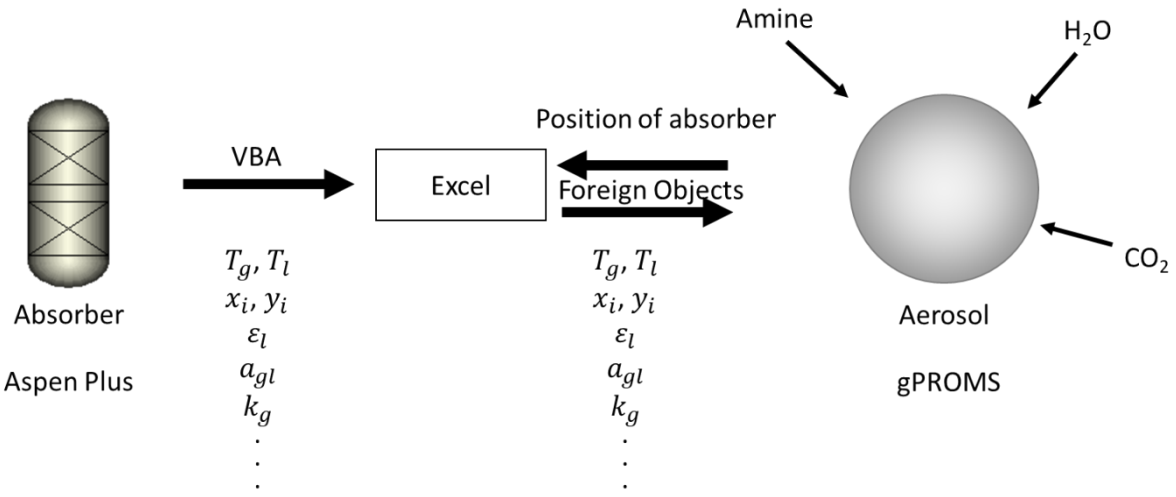

.Figure 1 Schematic of the connections between Aspen Plus and gPROMS.

2.2. Amine aerosol growth modeling

The amine aerosol growth model was modified from Kang et al. (2017) to apply for CO_2 absorption using MEA. Changes in the aerosol growth and amine composition, during the gas phase, were considered in the modified model. Mass transfer in the modified model was established based on the two-film theory to predict the aerosol growth. In the model, four components, including H_2O, CO_2, and MEA, were employed. For aerosol growth, material and energy balances are expressed as follows:

$$\frac{v_{drop}}{H_{col}}\frac{dn_{d,i}}{dh} = \frac{1}{v_{drop}} N_{gd,i} A_{gd} \quad (1)$$

$$\frac{v_{drop}}{H_{col}}\frac{dT_d}{dh} = \frac{Q_{gd} A_{gd}}{n_d C_{p,d}} \quad (2)$$

where i is the index of the component; h is the position of the aerosol in the absorber; $n_{d,i}$ is the mole number of specie i; v_{drop} is the average velocity of the droplets, which was assumed to be same as the gas velocity; H_{col} is the height of the column; $N_{gd,i}$ is the gas-aerosol mass transfer flux of specie i; and A_{gd} is the surface area of a droplet. Furthermore, T_d is the temperature of the aerosol phase; Q_{gd} is the heat transfer flux between the gas and aerosol phases; n_d is the total mole number of a droplet; and $C_{p,d}$ is the heat capacity. Since MEA and H_2O were the solvent components, the mass transfer flux $N_{gd,i}$ for H_2O and MEA is expressed as follows:

$$N_{gd,i} = \frac{k_{g,i}}{RT_g} \varphi \left(P_{g,i} - P^*_{d,i,corr}\right) \qquad for\ i = H_2O\ and\ MEA \quad (3)$$

For insoluble gas CO_2, the mass transfer flux, N_{gd,CO_2} should be modified as

$$N_{gd,CO_2} = k'_{g,CO_2}\left(P_{g,CO_2} - P^*_{d,CO_2,corr}\right) \quad (4)$$

where $k_{g,i}$ is the mass transfer coefficient for H_2O and MEA; φ is the Fuchs–Sutugin corrective factor; $P_{g,i}$ is the partial pressure of specie i, obtained from the absorber profile of Aspen Plus; $P^*_{d,i,corr}$ is the corrected equilibrium partial pressure of specie I; T_g is the temperature of the gas phase; R is the ideal gas constant. Furthermore, k'_{g,CO_2} is the enhanced mass transfer coefficient of CO_2 evaluated using the chemical reaction rates; it is defined as follows:

$$k'_{g,CO_2} = \frac{\sqrt{k_2 C^{free}_{MEA} D_{d,CO_2,mx}}}{H_{CO_2}} \quad (5)$$

where k_2 is the reaction rate constant of CO_2; C_{MEA}^{free} is the concentration of free MEA; $D_{d,CO_2,mx}$ is the CO_2 diffusivity of the mixture solution during the aerosol phase, and H_{CO_2} is the Henry law constant of CO_2.

Fuchs–Sutugin corrective factor φ was used for correcting the mass transfer rate for the micron-scale aerosol droplet. The Fuchs–Sutugin corrective factor is expressed as follows:

$$\varphi = \frac{0.75\alpha(1 + \mathrm{Kn})}{\mathrm{Kn}^2+\mathrm{Kn}+0.283\mathrm{Kn}\,\alpha+0.75\alpha} \quad (6)$$

The Knudsen number Kn is defined as follows:

$$Kn = \frac{2\lambda}{d_{drop}} \quad (7)$$

where α is the accommodation coefficient; λ is the mean free path of the surrounding fluid molecules; and d_{drop} is the diameter of an aerosol droplet.

The correction of vapor pressures for the droplets were also considered in the aerosol growth model because the vapor pressure of the curved surface was higher than the normal vapor pressure. Hence, in the aerosol model, Kelvin effect was used to correct the equilibrium partial pressure in a droplet. The corrected equilibrium partial pressure $P_{i,corr}^*$ is expressed as follows:

$$P_{d,i,corr}^* = P_{d,i}^* \exp\left(\frac{4\sigma v_{l,i}}{k_B T_{drop} d_{drop}}\right) \quad for\ i = MEA\ and\ H_2O \quad (8)$$

where $P_{d,i}^*$ is the equilibrium partial pressure of component i; σ is the surface tension between the gas and aerosol phases; $v_{l,i}$ is the partial molar volume of component i in the aerosol phase; k_B is the Boltzmann constant; T_{drop} is the temperature of the aerosol phase, and d_{drop} is the diameter of the aerosol.

The heat transfer flux Q_{gd} is expressed as follows:

$$Q_{gd} = N_{gd,H_2O}\Delta H_{H_2O} - N_{gd,MEA}\Delta H_{MEA} + N_{gd,CO_2}\Delta H_{CO_2} + h_g\left(T_g - T_d\right) \quad (9)$$

where ΔH_{H_2O}, ΔH_{MEA}, and ΔH_{CO_2} are the heat of vaporizations for H_2O and MEA and the heat of absorption for CO_2, respectively; h_g is the heat transfer coefficient; and T_g is the temperature of the gas phase.

The mass transfer coefficient $k_{g,i}$ for H_2O and MEA and the heat transfer coefficient h_g are calculated using the Sherwood number (Sh) and Nusselt number (Nu) assuming that the aerosols were spherical. The Sherwood and Nusselt numbers are expressed as follows:

$$Sh = 2 + 0.6\left(Re_g\right)^{\frac{1}{2}}\left(Sc_{g,i}\right)^{\frac{1}{3}} \quad (10)$$

$$\mathrm{Nu} = 2 + 0.6\left(\mathrm{Re_g}\right)^{\frac{1}{2}}\left(\mathrm{Pr}_g\right)^{\frac{1}{3}} \quad (11)$$

where Re_g is the gas Reynold number; $Sc_{g,i}$ is the gas Schmidt number for specie i; and Pr_g is the Prandtl number. However, in the absence of convection, Sherwood and Nusselt numbers can be considered to be 2. Hence, the mass transfer coefficient $k_{g,i}$ for H_2O and MEA is calculated as follows:

$$k_{g,i} = \frac{ShD_{g,i}}{d_{drop}} \quad (12)$$

The heat transfer coefficient is calculated as follows:

$$h_g = \frac{Nu\lambda_g}{d_{drop}} \quad (13)$$

where $D_{g,i}$ is the gas diffusion coefficient of specie i, obtained from the absorber profile of Aspen Plus; d_{drop} is the diameter of an aerosol droplet; and λ_g is the gas thermal conductivity.

The diameter of the droplets is calculated as follows:

$$d_{drop} = \frac{n_{d,i}}{\rho_{drop}/MW_{drop}} \quad (14)$$

where ρ_{drop} is the density of the aerosol droplets, and MW_{drop} is the molecular weight of the aerosol droplets. The equilibrium partial pressures during the aerosol phase $P^*_{d,i}$ is estimated based on the modified Raoult's law as follows:

$$P^*_{d,i} = \gamma_{d,i} x_{d,i} P^{sat}_{d,i} \quad for\ i = H_2O\ and\ MEA \quad (15)$$

where $P^*_{d,i}$ and $P^{sat}_{d,i}$ are the equilibrium and saturated partial pressures of H_2O and MEA during the aerosol phase, respectively; $\gamma_{d,i}$ is the activity coefficient; and $x_{d,i}$ is the mole fraction. The equilibrium partial pressures of CO_2 during the aerosol phase was obtained from the correlation (Xu and Rochelle, 2011).

In regard to the change in the gas phase, the change in MEA concentration in the gas phase was considered in the amine aerosol growth model, because the MEA concentration was significantly lower than H_2O and CO_2; this resulted in the mass transfer of MEA across the gas-aerosol interface, significantly affecting the gas phase MEA mole fraction. Compared to the other two components, change in the MEA composition caused by the gas-aerosol phase interaction may have been lower than that caused by the gas-liquid interaction. As a result, the MEA composition was re-calculated by considering both gas-aerosol and gas-liquid interactions. Furthermore, the mole fractions of N_2, H_2O, and CO_2 were obtained from the process modeling, using Aspen Plus. The MEA material balance can be simplified as a differential equation of the MEA partial pressure, dP_{MEA}, which is expressed as follows:

$$\frac{v_{drop}}{H_{col}} \frac{dP_{MEA}}{dh} = -\left(N_{gl,MEA} a_{gl} + N_{gd,MEA} A_d N_p\right) RT_g \quad (16)$$

where $N_{gl,MEA}$ is the mass transfer flux of MEA between the gas and liquid phases; a_{gl} is the gas-liquid contact area; N_p is the number of particle concentration, and R is the ideal gas constant.

This equation considers the mass transfers of gas-aerosol and gas-liquid interfaces. In the gas-aerosol mass transfer, a new term of PNC was introduced for estimating the total mass transfer flux from gas to aerosol in a column. The gas-liquid mass transfer flux of MEA $N_{gl,MEA}$ is expressed as follows:

$$N_{gl,MEA} = k_{g,MEA} \frac{\left(P_{g,MEA} - P^*_{l,MEA}\right)}{RT_g} \quad (17)$$

where $k_{g,MEA}$ is the gas mass transfer coefficient of MEA for the gas-liquid interface, obtained from the absorber profile of Aspen Plus. $P_{g,MEA}$ is the partial pressure of MEA, and $P^*_{l,MEA}$ is the equilibrium partial pressure of MEA for the liquid phase, obtained from the absorber profile of Aspen Plus.

2.3. Physical properties

Thermodynamic properties and mass transfer parameters of the gas and liquid phases were obtained from the absorber model, using the Excel interface. The thermodynamic properties of the aerosol phase, such as activity coefficients, heat capacity, surface tension, and true composition, were obtained from the Aspen Properties database, using the electrolyte non-random-two-liquid (e-NRTL) model for MEA through CAPE-OPEN Thermo-interface to connect gPROMS. A few missing parameters were included based on literature, such as vapor pressure and diffusion coefficient for the aerosol phase. The values of these properties are listed in **错误!未找到引用源。**.

Table 1. Summaries of the sources of thermodynamic properties and mass transfer parameters.

From Excel	T_g, $x_{l,i}$, ρ_g, λ_g, $D_{g,i}$,ν_g,$K_{g,i}$, a_{gl}, $\gamma_{l,i}$, $P^*_{l,MEA}$
From Cape-Open	$\gamma_{d,i}$, σ_{drop}, $C_{p,d}$,$x_{true,d,i}$
From Empirical equations	
D_{d,CO_2} (Kang et al., 2014)	$\dfrac{2.35\times10^{-6}\exp\left(-\frac{2119}{T_d}\right)}{5.07\times10^{-6}\exp\left(-\frac{2371}{T_d}\right)}D_{N_2O}$
	$D_{N_2O}=\left(\begin{matrix}\left(5.07+0.865C_{d,MEA}+0.278C_{d,MEA}^2\right)\\ \times\exp\left(\dfrac{-2371-93.4C_{d,MEA}}{T_d}\right)\end{matrix}\right)$
$P^{sat}_{d,MEA}$ (AspenTech, 2013)	$\exp\left(172.78-\dfrac{13492}{T_d}-21.914*log(T_d)+1.38\times10^{-5}T_d^2\right)$
P^{sat}_{d,H_2O} *(AspenTech, 2013)*	$\exp\left(72.55-\dfrac{7206.7}{T_d}-7.1385*log(T_d)+4.05\times10^{-6}T_d^2\right)$
P^*_{d,CO_2} (Xu and Rochelle, 2011)	$\exp\left(38.6+\left(\dfrac{-12379}{T_d}\right)-16.0LDG_d^2+3556\left(\dfrac{LDG_d}{T_d}\right)+8702\left(\dfrac{LDG_d^2}{T_d}\right)\right)$

2.4. Amine absorber modeling by Aspen Plus

The rate-based absorber was modeled using the example model provided by AspenTech (2013), employing a rigorous e-NRTL thermodynamic framework and rigorous kinetics with reactions. Models for the mass transfer and interfacial area were based on Onda et al. (1968), and the liquid holdup was based on Stichlmair et al. (1989). The number of stages for the absorber was set to 100, to export more smoother profiles.

3. Experiments

错误!未找到引用源。 shows the experimental flowsheet employed in this study. A lab-scale packed-bed absorber (Liu et al., 2015) was used to carry out the experiment for validating the aerosol growth. The equipment contained four parts of removable glass packed sections. In each part of the packed section, the inner diameter and height were 25.4 and 300 mm, respectively. In this study, only one packed section was used for investigating CO_2 removal and the aerosol size. The plastic Raschig rings fully filled the packed section. The porosity and packing surface area were 0.86 and 610 m^2/m^3, respectively. The liquid flow was 0.2 L/min and inlet gas flows were 1.5 and 3 L/min. The inlet flow containing 20% CO_2 and 80% N2 passed through a solution and an aerosol generator (Model 3076, TSI) to carry the aerosol into the absorber. The solution added sucrose instead of sulfuric acid as the nuclei of the aerosol. Usage of the sucrose aqueous solution prevented the erosion of the detection equipment. Sucrose is a non-volatile solute which provides a condensed nucleus during the atomization process and produces the aerosol with stable size distribution due to its fixed velocity when passing through an atomizer (Kaufman, 2000; Lee et al., 2016). Optical particle sizer (Model 3330, TSI) was used for measuring the aerosol particle size distribution (PSD) and PNC at the inlet and outlet of the gas. The particle sizer could measure 0.3 to 10 μm of particle size. The PNC range of the particle sizer was 0 to 3000 #/cm^3. To prevent an over PNC limitation, an aerosol diluter (Model 3332, TSI) was installed between the particle sizer and gas flows. The dilution ratio of the aerosol diluter was 1/100. The detailed operating conditions are shown in 错误!未找到引用源。.

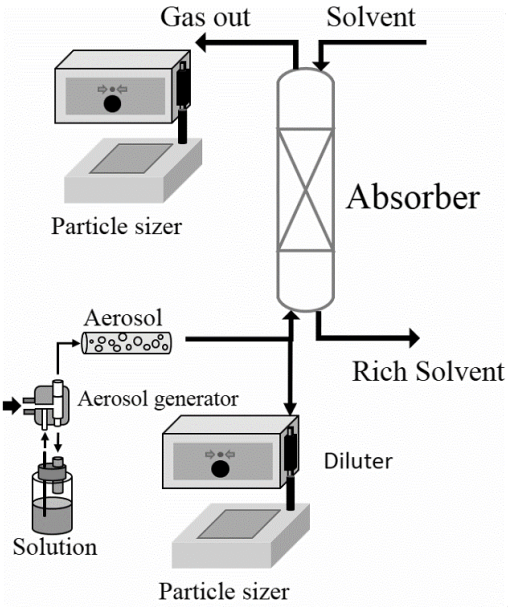

Figure 2. Schematic diagram of the experimental flowsheet.

Table 2. Operating conditions of the lab-scale absorber.

	Absorber
Packing Height (cm)	30

Diameter (cm)	2.54
Packing type	Plastic Raschig Rings
Packing surface area (m^2/m^3)	610
Lean solvent T (°C)	30
Liquid flow rate(L/min)	0.2
MEA concentration (wt%)	30
Gas inlet T (°C)	30
Gas flow rate(L/min)	1.5/3
Inlet CO_2	20%
Inlet N_2	80%

4. Results and Discussions

4.1. Investigation of the experiment

错误!未找到引用源。 shows the distribution of the inlet aerosol particle size with different sucrose concentrations. The PNCs were found to be 200, 100, and 70 thousand of #/cm^3. Due to the limitation of the equipment, the particle sizes were observed from 0.3 to 10 um. As shown in Figure 3, most particles were found to be less than 0.3 um in size. **错误!未找到引用源。** shows the distribution of the outlet aerosol particle sizes. Compared to the inlet aerosol particle sizes, the average size of the outlet aerosol was found to be 1.38 μm and the PNC was observed to be approximately $3.3 \times 10^5\ \#/cm^3$.

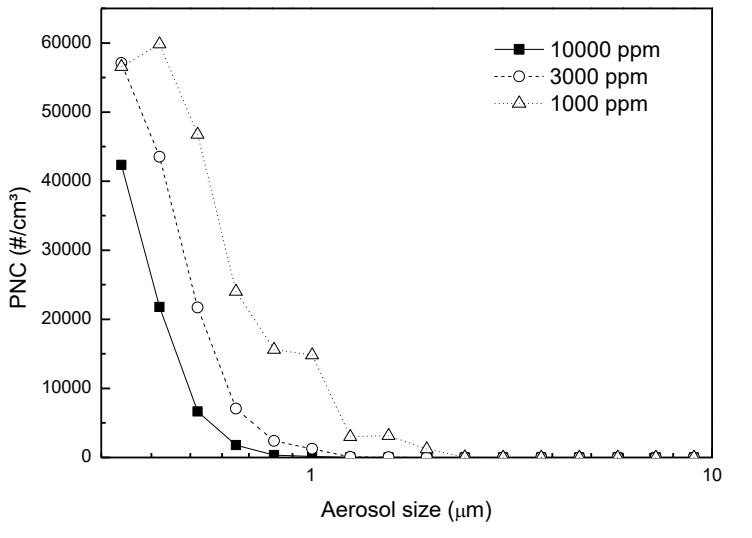

Figure 3. PSD and PNC of the inlet gas flow.

Preprints (www.preprints.org) | NOT PEER-REVIEWED | Posted: 5 July 2020 doi:10.20944/preprints202007.0043.v1

Peer-reviewed version available at Environments 2020, 7, 58; doi:10.3390/environments7080058

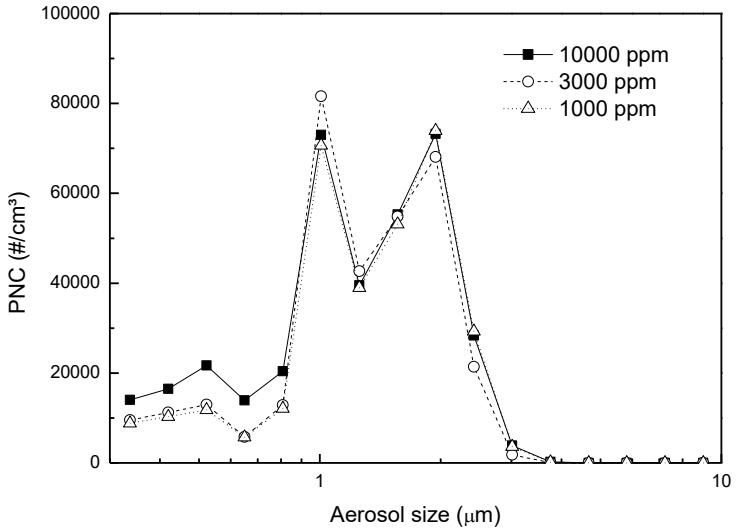

Figure 4. PSD and PNC of the outlet gas flow.

4.2. Validation of the absorber and aerosol growth model

错误!未找到引用源。 shows that the absorber model could predict the outlet CO_2 mole fraction of the experimental data with 1.5 and 3 L/min gas flow rate. Results of the absorber model were found to be in good agreement with the experimental data, with an average error percentage of 3.2%. **错误!未找到引用源。** shows that the aerosol growth model could predict the average outlet aerosol size after adjusting the accommodation coefficient α. When α was adjusted to 0.025, the aerosol growth model could predict the aerosol size.

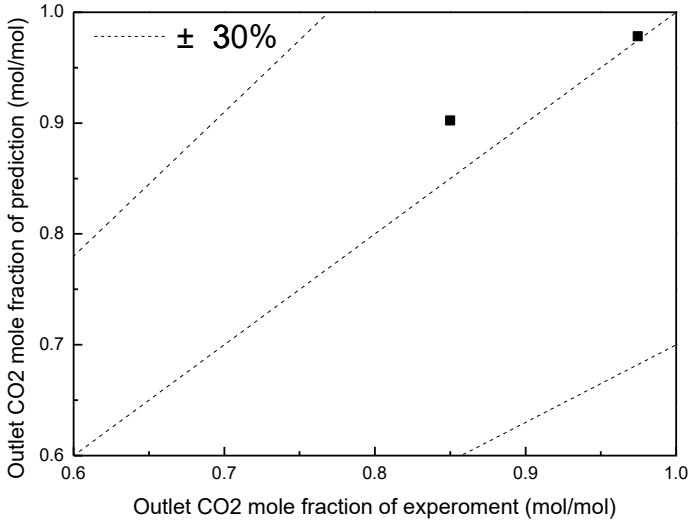

Figure 5. Agreement of the CO_2 outlet mole fraction between the absorber model and experimental data of the absorber.

Preprints (www.preprints.org) | NOT PEER-REVIEWED | Posted: 5 July 2020 doi:10.20944/preprints202007.0043.v1

Peer-reviewed version available at Environments 2020, 7, 58; doi:10.3390/environments7080058

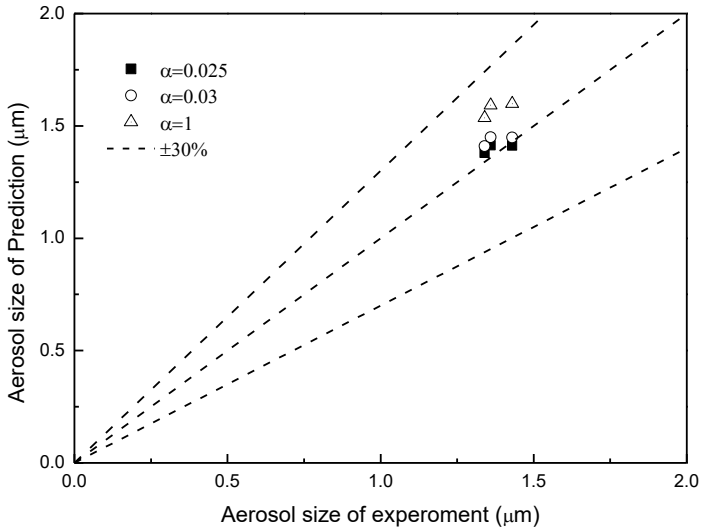

Figure 6. Agreement of the outlet aerosol size between the aerosol growth model and experimental data of the aerosol with different accommodation coefficients α.

4.3. Effect of PNC for aerosol growth

错误!未找到引用源。 shows the aerosol growth in the absorber, using different PNCs and 0.025 of α. As shown in the figure, the final aerosol size decreased as the PNC increased, because a high PNC decreased the driving force of MEA to inhibit the aerosol growth rate. **错误!未找到引用源。** shows the contours of the aerosol. PNC was observed to be the main factor affecting the aerosol growth, whereas initial aerosol size only slightly affected the growth.

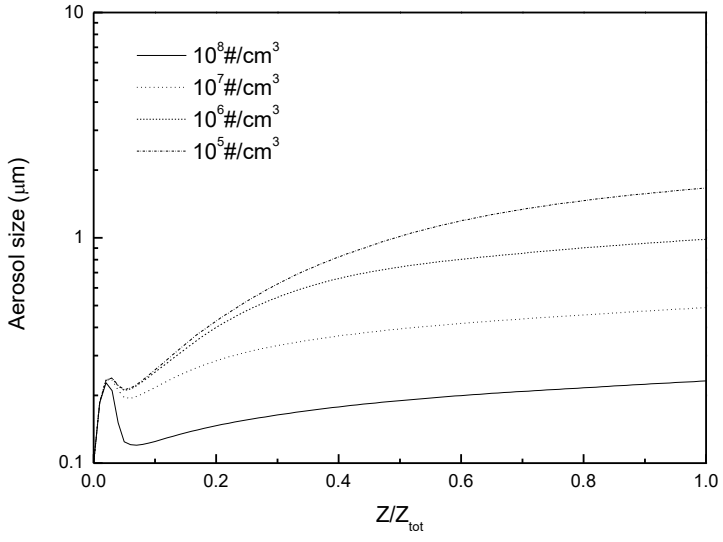

Figure 7. Aerosol size profile in the absorber with different PNCs observed using aerosol growth model.

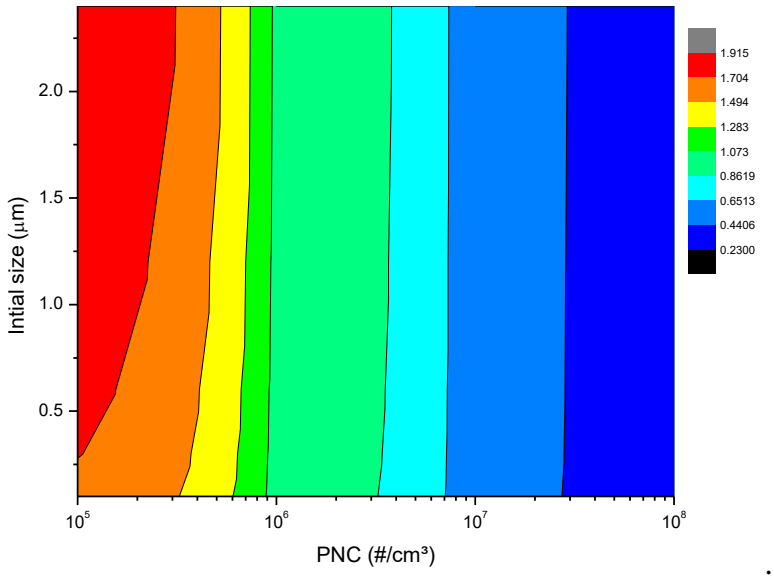

Figure 8. Contours of the outlet aerosol sizes with different initial aerosol sizes and PNCs.

4.4. Effect of PNC on MEA emission

错误!未找到引用源。 shows the MEA emissions by computing the MEA concentrations of the gas and aerosol phases. Results showed that the MEA emission increased as the PNC increased. An emission of 300 mg/m^3 was observed at the PNC of 10^8#/cm^3, which tripled compared to the PNC of 0 #/cm^3. **错误!未找到引用源。** shows the contours of the MEA emissions and it can be observed that PNC was the main factor to carry out MEA from the absorbers. The initial size of the aerosol was also observed to have an effect when the PNC was below 10^7 #/cm^3

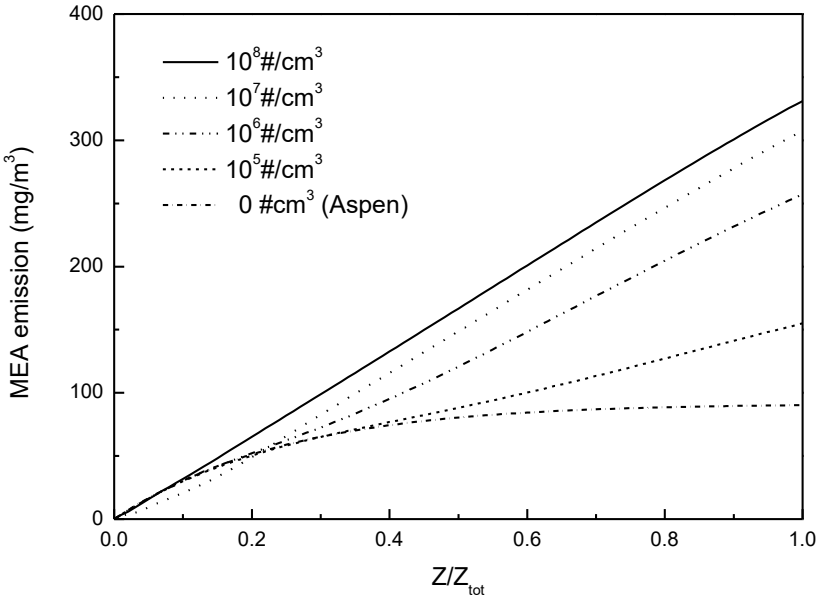

Figure 9. Total MEA concentration profile of the gas phase in the absorber with different PNCs using the aerosol growth model.

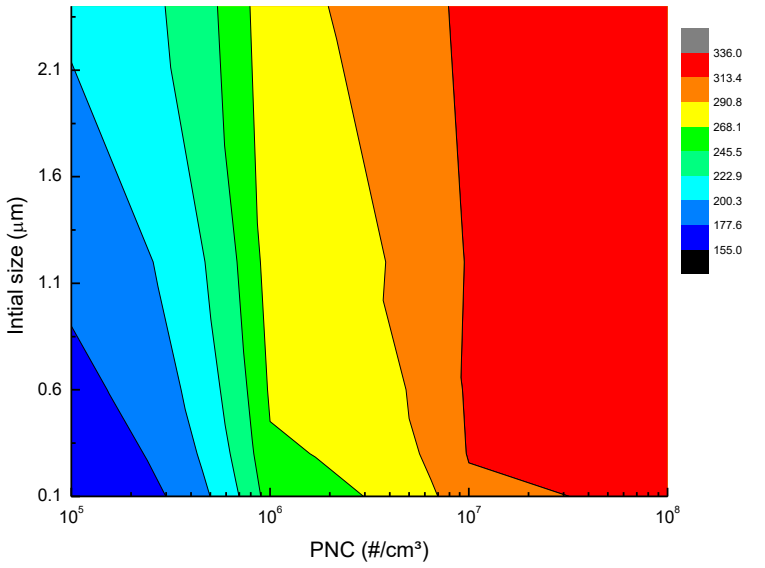

Figure 10. Contours of MEA emissions with different initial aerosol sizes and PNCs.

5. Conclusions

In this study, we built an MEA aerosol growth model that incorporated the effect of PNC, between the aerosol and gas phases, on the aerosol growth and we carried out an experiment to measure the aerosol particle size. In the experiment, sulfuric acid was replaced with sucrose as the nuclei of the aerosol to prevent the corrosion of the equipment. Experimental results showed that the inlet aerosol sizes were smaller than 0.3 μm and the outlet aerosol size increased to 1. 38 μm with a PNC of 3.3×10^5 #/cm³. The aerosol growth model was validated with the in-house experimental data. After adjusting the accommodation coefficient to 0.025, the aerosol growth model was able to predict the aerosol size. PNC was observed to be the main factor affecting the aerosol growth and MEA emission. When the PNC increased, the aerosol size was observed to decrease, while the MEA emission was observed to increase.

Acknowledgment

The authors acknowledged the financial support provided by Ministry of Science and Technology through the grant MOST 107-3113-E-007-002.

Reference

AspenTech, 2013. Rate-based model of the CO_2 capture process by MEA using Aspen Plus.

Brachert, L., Mertens, J., Khakharia, P., Schaber, K., 2014. The challenge of measuring sulfuric acid aerosols: number concentration and size evaluation using a condensation particle counter (CPC) and an electrical low pressure impactor (ELPI+). Journal of aerosol science 67, 21-27.

Bradie, J., Dickson, A., 1969. Removal of Entrained Liquid Droplets by Wire-Mesh Demisters, Proceedings of the Institution of Mechanical Engineers, Conference Proceedings. SAGE Publications Sage UK: London, England, pp. 195-203.

Dave, N., Do, T., Jackson, P., Feron, P., Azzi, M., Attalla, M., 2010. CO 2 Capture Mongstad-Project B Theoretical evaluation of the potential to form and emit harmful compounds, Task 1: Process Chemistry. The Commonwealth Scientific and Industrial Research Organisation (CSIRO) Report, Australia.

El-Dessouky, H.T., Alatiqi, I.M., Ettouney, H.M., Al-Deffeeri, N.S., 2000. Performance of wire mesh mist eliminator. Chemical Engineering and Processing: Process Intensification 39, 129-139.

Fine, N.A., Goldman, M.J., Nielsen, P.T., Rochelle, G.T., 2013. Managing n-nitrosopiperazine and dinitrosopiperazine. Energy procedia 37, 273-284.

Fulk, S.M., Chen, E., Rochelle, G.T., 2015. Aerosol Mitigation in Amine-Based CO2 Capture, 2nd Post Combustion Capture Conference (PCCC2).

Kamijo, T., Kajiya, Y., Endo, T., Nagayasu, H., Tanaka, H., Hirata, T., Yonekawa, T., Tsujiuchi, T., 2013. SO 3 impact on amine emission and emission reduction technology. Energy Procedia 37, 1793-1796.

Kang, J.-L., Sun, K., Wong, D.S.-H., Jang, S.-S., Tan, C.-S., 2014. Modeling studies on absorption of CO_2 by monoethanolamine in rotating packed bed. International Journal of Greenhouse Gas Control 25, 141-150.

Kang, J.-L., Zhang, Y., Fulk, S., Rochelle, G.T., 2017. Modeling amine aerosol growth in the absorber and water wash. Energy Procedia 114, 959-976.

Kaufman, S.L., 2000. Electrospray diagnostics performed by using sucrose and proteins in the gas-phase electrophoretic mobility molecular analyzer (GEMMA). Analytica Chimica Acta 406, 3-10.

Khakharia, P., Brachert, L., Mertens, J., Anderlohr, C., Huizinga, A., Fernandez, E.S., Schallert, B., Schaber, K., Vlugt, T.J., Goetheer, E., 2015. Understanding aerosol based emissions in a Post Combustion CO 2 Capture process: Parameter testing and mechanisms. International Journal of Greenhouse Gas Control 34, 63-74.

Lee, F.-C., Lu, Y.-F., Chou, F.-C., Cheng, C.-F., Ho, R.-M., Tsai, D.-H., 2016. Mechanistic study of gas-phase controlled synthesis of copper oxide-based hybrid nanoparticle for CO oxidation. The Journal of Physical Chemistry C 120, 13638-13648.

Liu, J., Gao, H.-C., Peng, C.-C., Wong, D.S.-H., Jang, S.-S., Shen, J.-F., 2015. Aspen Plus rate-based modeling for reconciling laboratory scale and pilot scale CO_2 absorption using aqueous ammonia. International Journal of Greenhouse Gas Control 34, 117-128.

Mertens, J., Brachert, L., Desagher, D., Thielens, M., Khakharia, P., Goetheer, E., Schaber, K., 2014. ELPI+ measurements of aerosol growth in an amine absorption column. International Journal of Greenhouse Gas Control 23, 44-50.

Onda, K., Takeuchi, H., Okumoto, Y., 1968. Mass transfer coefficients between gas and liquid phases in packed columns. Journal of chemical engineering of Japan 1, 56-62.

Stichlmair, J., Bravo, J., Fair, J., 1989. General model for prediction of pressure drop and capacity of countercurrent gas/liquid packed columns. Gas Separation & Purification 3, 19-28.

Thitakamol, B., Veawab, A., Aroonwilas, A., 2007. Environmental impacts of absorption-based CO 2 capture unit for post-combustion treatment of flue gas from coal-fired power plant. International Journal of Greenhouse Gas Control 1, 318-342.

Xu, Q., Rochelle, G., 2011. Total pressure and CO2 solubility at high temperature in aqueous amines. Energy Procedia 4, 117-124.